Advances in Atmospheric Sciences
Impact Factor: 3.158
E-alert
ISSN 0256-1530
CN 11-1925/O4

**Objective Identification and Climatic Characteristics of Heavy-Precipitation Northeastern China Cold Vortexes**

Xu CHEN, Xiaoyong ZHUGE, Xidi ZHANG, Yuan WANG, Daokai XUE

**Citation:** Chen, X., X. Y. Zhuge, X. D. Zhang, Y. Wang, and D. K. Xue 2023: Objective Identification and Climatic Characteristics of Heavy-Precipitation Northeastern China Cold Vortexes, *Adv. Atmos. Sci.*, 40, 305-316. doi: 10.1007/s00376-022-2037-y.

View online: https://doi.org/10.1007/s00376-022-2037-y

ADVANCES IN ATMOSPHERIC SCIENCES, VOL. 40, FEBRUARY 2023, 305–316

• **Original Paper** •

# Objective Identification and Climatic Characteristics of Heavy-Precipitation Northeastern China Cold Vortexes

Xu CHEN[1], Xiaoyong ZHUGE[*2], Xidi ZHANG[1,3], Yuan WANG[1], and Daokai XUE[1]

[1]*Key Laboratory of Mesoscale Severe Weather of Ministry of Education, and School of Atmospheric Sciences, Nanjing University, Nanjing* 210023, *China*

[2]*Key Laboratory of Transportation Meteorology of China Meteorological Administration, Nanjing Joint Institute for Atmospheric Sciences, Nanjing* 210041, *China*

[3]*National Meteorological Center, Beijing* 100081, *China*

(Received 13 February 2022; revised 14 May 2022; accepted 30 June 2022)

ABSTRACT

The northeastern China cold vortex (NCCV) plays an important role in regional rainstorms over East Asia. Using the National Centers for Environmental Prediction Final reanalysis dataset and the Global Precipitation Measurement product, an objective algorithm for identifying heavy-precipitation NCCV (HPCV) events was designed, and the climatological features of 164 HPCV events from 2001 to 2019 were investigated. The number of HPCV events showed an upward linear trend, with the highest frequency of occurrence in summer. The most active region of HPCV samples was the Northeast China Plain between 40°–55°N. Most HPCV events lasted 3–5 days and had radii ranging from 250 to 1000 km. The duration of HPCV events with larger sizes was longer. About half of the HPCV events moved into (moved out of) the definition region (35°–60°N, 115°–145°E), and half initiated (dissipated) within the region. The initial position was close to the western boundary of the definition region, and the final position was mainly near the eastern boundary. The locations associated with the precipitation were mostly concentrated within 2000 km southeast of the HPCV systems, and they were farther from the center in the cold season than in the warm season.

**Key words:** northeastern China cold vortex, heavy precipitation, objective identification, climatological features

**Citation:** Chen, X., X. Y. Zhuge, X. D. Zhang, Y. Wang, and D. K. Xue, 2023: Objective identification and climatic characteristics of heavy-precipitation northeastern China cold vortexes. *Adv. Atmos. Sci.*, **40**(2), 305–316, https://doi.org/10.1007/s00376-022-2037-y.

**Article Highlights:**

- The number of heavy-precipitation northeastern China cold vortex (HPCV) events showed an upward linear trend from 2001–19.
- Most HPCV events lasted 3–5 days and had radii ranging from 250 to 1000 km.
- Precipitation was mostly concentrated within 2000 km southeast of the HPCV centers.

## 1. Introduction

Cut-off lows are isolated, closed cyclonic eddies with a cold core or cold trough in the mid- to high-latitude westerly winds. They have detached from a deep trough due to warm air masses cutting off their connection with colder air to the north (Hsieh, 1949; Palmén, 1949; Gimeno et al., 2007). There are three preferred regions of cut-off-low occurrences in the Northern Hemisphere: the southern European and eastern Atlantic coasts, the eastern North Pacific, and the northern China–Siberian section of the northwestern Pacific coast (Nieto et al., 2005). Cut-off lows over Northeast China are usually called northeastern China cold vortexes (NCCVs).

The current widely-used definition of NCCV events is proposed by Zheng et al. (1992) and Sun et al. (1994). An NCCV event should meet the following three criteria: (1) a low-pressure system accompanied by a cold core or an evident cold trough with at least one closed geopotential height contour at the 500-hPa isobaric surface; (2) the low-pressure system, as defined in the first criteria, is located within the region (35°–60°N, 115°–145°E); (3) the defined low-pressure system must last for three or more days within the study region.

* Corresponding author: Xiaoyong ZHUGE
Email: xyzhuge@yeah.net

According to the definition above, the identification of NCCVs focuses on the configuration of the geopotential height and temperature fields, as well as the continuity of the system. These are the issues surrounding the design of an objective algorithm. Zhang et al. (2008) detected NCCV events only based on the geopotential height field, ignoring the influence of the temperature field. Hu et al. (2010) designed a three-step method with a positive zonal temperature Laplacian constraint. However, this method does not work well with different spatial resolutions of data. Nieto et al. (2005) and Wang et al. (2012) introduced a thermal front parameter (TFP, $\mathrm{TFP} = -\nabla|\nabla T|\cdot(\nabla T/|\nabla T|)$). This formula is complicated and difficult to attain. In addition to the geopotential height and temperature fields, Jiang et al. (2012), Wang et al. (2012), and Huang and Li (2020) took the wind field into account. As cut-off lows are quasi-geostrophic in the mid- to high latitudes and the low-pressure center is basically equivalent to the cyclonic center, it is therefore not necessary to consider the wind field.

A tracking procedure is performed to detect whether NCCVs are newly generated or just the same system as the previous time step. There are no definite rules for NCCV tracking, and researchers have designed different algorithms based on their own experiences. In the algorithm of Zhang et al. (2008), if two NCCV centers were within three grid points at adjacent times and the radial difference was $\leqslant$ 500 km, they belonged to the same system. Hu et al. (2010) proposed that two NCCVs were regarded as the same system only if the speed of movement was < 10° long. /6 h. Wang et al. (2012) employed a method different from that of Hu et al. (2010); for any two consecutive days, if the longitude and latitude differences of NCCV centers were within (–10°, 10°) and (–7.5°, 7.5°) respectively, they belonged to the same system. Similar to Wang et al. (2012), the algorithm of Huang and Li (2020) was that the meridional distance at any two consecutive synoptic hours was $\leqslant$ 5° and the zonal distance was $\leqslant$ 5° to the west ($\leqslant$ 10° to the east).

Persistent NCCV activities have contributed to the increase of regional rainstorms in Northeast China (Sun et al., 2000; Xie et al., 2012). When an NCCV system is baroclinic, the cold center lags behind the geopotential height center in the mid-to upper-troposphere (e.g., 500 hPa), leading to cold advection behind the vortex. An unstable stratification will be established if the air in the lower layers is warm and moist, which is necessary for heavy precipitation (Zhang and Li, 2009). Bai and Sun (1997) showed that 87.5% of NCCVs with strong convection had obvious water vapor transport and convergence. The precipitation mainly falls in the southeastern quadrant of the system (Sun et al., 2002). This is because the east side of the cold vortex has positive vorticity advection, which excites updrafts, and also because the warm and cold air also usually meets here, making it easier to trigger severe convective weather (Hsieh, 1949). In addition, regional rainstorms mainly occur in the development and maintenance stage of the cold vortex, when the system is strongly baroclinic. However, in the generation and maturity stage, the amount of precipitation is small, yet sometimes there is convective weather such as thunderstorms (Sun et al., 1995; Ying et al., 2014).

An NCCV accompanied by heavy rainfall, namely a heavy-precipitation NCCV (HPCV), is a disastrous weather system worthy of attention. Sun et al. (2002) first proposed a criterion to distinguish HPCVs from NCCVs: among 95 stations covering Northeast China (Liaoning, Jilin, and Heilongjiang Provinces) and eastern Inner Mongolia (east of 115°E), at least three stations have the records of daily rainfall $\geqslant$ 50 mm from 1200 UTC to next 1200 UTC. However, Sun et al. (2002) only focused on HPCVs in Northeast China, and the precipitation datasets they used came from weather stations in the surface meteorological observing network, with limited resolution and coverage. In this study, a precipitation dataset with better temporal (30 min) and spatial (0.1° × 0.1°) resolution and larger coverage, called the Integrated Multi-satellite Retrievals for Global Precipitation Measurement (IMERG) project, was used. Previous studies mostly focused on the statistical characteristics of NCCVs (Sun et al., 1994; Zhang et al., 2008; Hu et al., 2010), and the features of HPCVs are still not well understood. Therefore, it is necessary to investigate the climatological characteristics of HPCVs with finer datasets to deepen the understanding of heavy rain over northeast China and its vicinity.

The remainder of this article is organized as follows. Section 2 introduces the data and method for objectively identifying HPCV samples and events. Section 3 describes the distribution characteristics of HPCVs. Section 4 analyzes four types of HPCV events based on their positions. Section 5 shows the characteristics of HPCV samples related to precipitation. Conclusions and discussions are given in section 6.

## 2. Data and Methodology

For the objective identification of NCCVs and HPCVs, the U.S. National Centers for Environmental Prediction (NCEP) Final operational global reanalysis, i.e., the NCEP Final dataset (NCEP_FNL; Kalnay et al., 1996), with a spatial resolution of 1.0° × 1.0° was used. The NCEP_FNL data are available at four synoptic times daily (i.e., 0000, 0600, 1200, and 1800 UTC). HPCV events are selected from the NCCV ones based on the IMERG precipitation dataset.

Available from June 2000, the IMERG dataset has three types of products (Early, Late, and Final). Compared with the other two products, the Final product uses monthly gauge data to create research-level products and performs better than the others (Yang et al., 2020). There are two types of precipitation datasets in the Final product: precipitationCal (with gauge-adjusted processes) and precipitationUnCal (without gauge-adjusted processes). Existing studies showed that the IMERG precipitationCal dataset is capable of capturing the basic characteristics of precipitation, especially at 12-hourly and daily scales (Huang et al., 2018; Hosseini-Moghari and Tang, 2022). Guo et al. (2016) also pointed out that the IMERG precipitationCal dataset has

less bias in estimating changes in precipitation over the Chinese mainland. Therefore, the precipitationCal dataset was used to identify HPCVs.

### 2.1. *Algorithm for Identifying NCCV Samples and Events*

Following the definition of Zheng et al. (1992) and Sun et al. (1994), the automated algorithm is designed as follows.

(1) A grid point is considered a candidate NCCV center if its 500-hPa geopotential height is lower than that of the neighboring eight grid points. As most NCCVs have maximum radii ⩽ 1500 km (Hu et al., 2010), the study region (35°–60°N, 115°–145°E) is extended temporarily outward by 15°—that is, (20°–75°N, 100°–160°E) to ensure the positioning accuracy of the NCCV centers near boundaries.

(2) If multiple candidate NCCV centers exist in a 10° × 10° grid box, then the grid point with the lowest geopotential height is retained, and others are ruled out. At the same time, detected points that are not in the study region (35°–60°N, 115°–145°E) are discarded.

(3) For the area surrounding the candidate NCCV center with a radius of 1500 km, the temperature centroid (the mean latitude and longitude weighted by $T$, where $T$ is equivalent to 300 K minus the 500-hPa temperature) is calculated. The candidate NCCV center can be regarded as an NCCV center if the distance between it and the temperature centroid is ⩽ 500 km.

(4) Similar to the tracking algorithm of Huang and Li (2020), the NCCV centers at any two consecutive synoptic hours belong to the same system if the meridional distance is ⩽ 5° and the zonal distance is ⩽ 5° to the west (⩽ 10° to the east). If multiple centers fit the criteria, then we take the nearest pair. The NCCV events must last for at least 12 synoptic hours (i.e., three days). In an NCCV event, the NCCV at a certain synoptic hour is defined as an NCCV sample.

(5) The fake NCCV events caused by the extratropical transition of typhoons are removed by using the best track dataset from the Shanghai Typhoon Institute, Chinese Meteorological Administration. The NCCV event is fake if the distance between the NCCV center and the typhoon center is ⩽ 500 km for at least three synoptic hours.

To measure the size of an NCCV sample, a definition similar to Wen et al. (2018) and Guo et al. (2021) is adopted. The radius of an NCCV sample is defined as the distance between the NCCV center and the outermost closed 4-dagpm-interval geopotential height contour.

### 2.2. *Algorithm for Identifying HPCV Samples and Events*

The composite analysis of the heavy precipitation associated with the NCCV samples from 2019 is shown in Fig. 1. The rainfall distribution is comma-shaped and mainly to the south and east of the composite cold vortex. A large area of precipitation can be included for the dashed red box that extends 10° to the south and east from the dashed blue rectangle (the external rectangle around the outermost closed contour). The region covered by the dashed red rectangle is referred to here as the cold vortex rain area. Notably, some NCCV samples lack a closed 4-dagpm-interval geopotential height contour, especially when they dissipate or move out of the study region. At this time, no attention is paid to the cold vortex rain area.

Because the earliest available IMERG data is from June 2000, the HPCV events are identified during the time period 2001–19. Based on the analysis in Fig. 1, the 24-h accumulated precipitation of an NCCV sample is calculated by the amount of rainfall in the ±12 h time period over the cold vortex rain area; then, a new criteria of HPCV events based on the high resolution of IMERG dataset instead of station rainfall records by Sun et al. (2002) can be designed as follows.

(1) The grid points with 24-h accumulated precipitation > 0 mm are stored as a list $\boldsymbol{N}$ at a certain synoptic hour. Then $\boldsymbol{N}$ is sorted in descending order, and the average value of the first 10% elements is calculated as $P$. The total number of grid points with 24-h accumulated precipitation ⩾ 50 mm is defined as $S$. If the conditions are such that $P$ is ⩾ 50 mm and $S$ is ⩾ 1000, the NCCV sample at this synoptic hour can be defined as an HPCV sample.

(2) If at least one HPCV sample can be found in an NCCV event, this NCCV event is defined as an HPCV event.

Note that the identification algorithm for HPCV events proposed in this study differs from that of Sun et al. (2002). The main discrepancy between the two methods is their coverage. Sun et al. (2002) only focused on the HPCVs affecting Northeast China. However, the active regions of HPCVs also include the Russian Far East and the Japanese islands

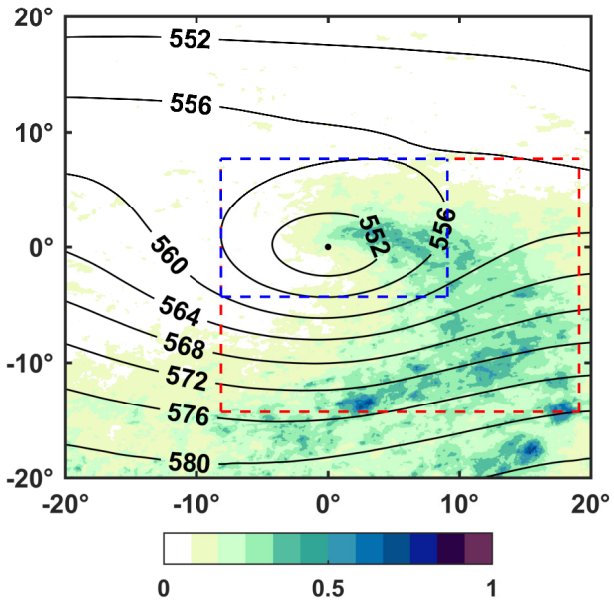


**Fig. 1.** Composites of the IMERG precipitation (shading; units: mm $h^{-1}$) and 500-hPa geopotential height (black contours; units: dagpm). The contour interval is 4 dagpm. The dashed blue box indicates the external rectangle around the outermost closed contour of the composite cold vortex. The dashed red rectangle defines the cold vortex rain area.

and their adjacent sea areas. Therefore, the definition of HPCV events by our algorithm is more credible.

Using the two algorithms above, a total of 472 NCCV events and 164 HPCV events are identified, which means that about 34.75% of the NCCV events are defined as an HPCV.

## 3. Distribution Characteristics of HPCVs

This section presents the temporal and spatial characteristics of HPCV samples and events, including their duration and size. Spring refers to March–May (MAM), summer is June–August (JJA), autumn is September–November (SON), and winter is December–February (DJF).

### 3.1. *Temporal Variations*

HPCVs occurred more often in summer, with an average number of eight samples and 1.5 events per month. They are less common in the cold season, especially from February to April (Fig. 2). The sufficient supply of low-level moisture in summer is conducive to unstable stratification, triggering convection and precipitation. More details are discussed in Section 5. The ratio of HPCV to NCCV, in terms of samples and events, is higher from August to October. In contrast, this proportion is lower than 10% from February to April.

On average, HPCV events occur about nine times annually, consisting of 39 HPCV samples. The standard deviation of the annual number of HPCV samples and events is 14.9 and 2.8, respectively, implying that the occurrence of HPCVs has a considerable inter-annual variability. There were 14 HPCV events and 68 HPCV samples in 2012, whereas only 4 HPCV events occurred in 2011, along with the lowest amount of samples (16 HPCV samples). The largest year-to-year variation appears over these two years.

Note that the number of HPCV samples and events show an upward linear trend from 2001 to 2019. In fact, the number of NCCV samples and events also shows an upward linear trend within the same period (see Fig. S1 in the electronic supplementary material). The upward trend of HPCVs has not been studied yet. One possible reason for the upward trend of NCCVs is global warming. Ma and Zhu (2022) found that the Bering Sea ice concentrations are reduced due to global warming. As a result, a tripolar anomalous sea surface temperature pattern in the North Atlantic develops, which excites the Rossby wave train. Zhang et al. (2016) demonstrated that the polar vortex area in the Eurasian continent had increased significantly, and the vortex center during the 2000s shifted further southward than before. When the connection between the polar vortex and the cold air is cut off, a cut-off low is formed. Therefore, an active polar vortex is conducive to the increased occurrences of NCCV events.

### 3.2. *Spatial Distribution*

To better describe the characteristics of HPCV samples, the spatial distributions of general NCCV samples are given

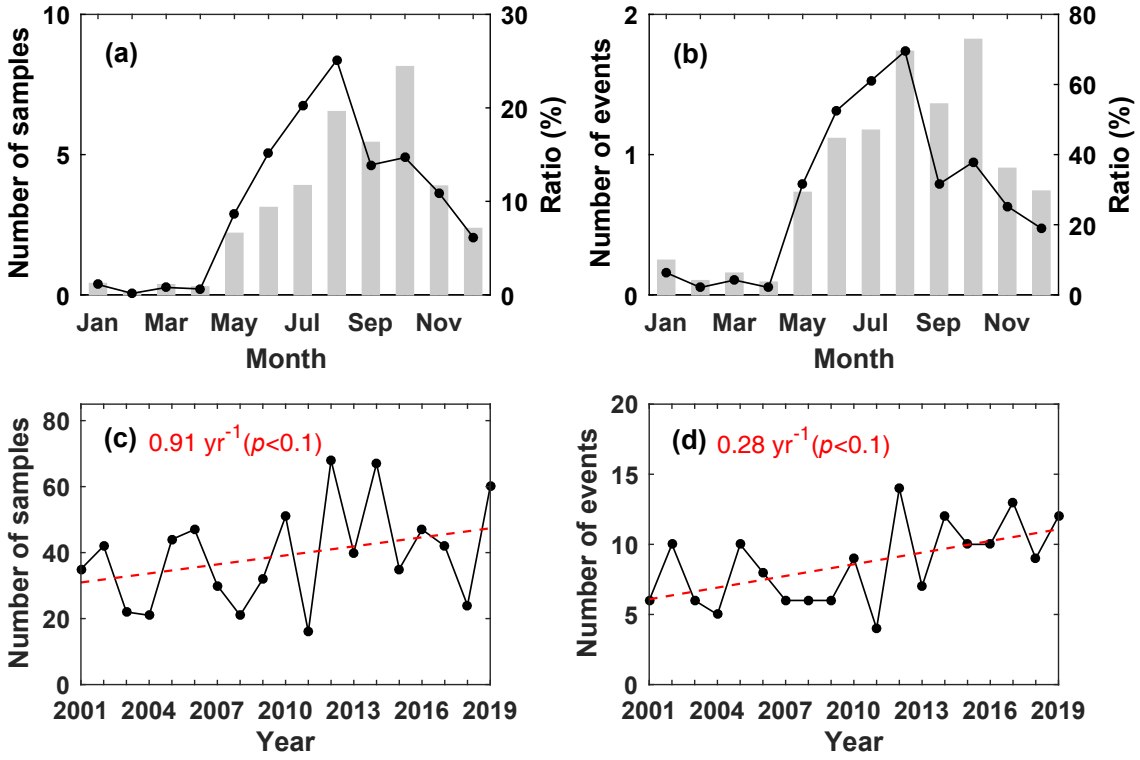


**Fig. 2.** (a–b) Monthly and (c–d) yearly variations of the number of HPCV (a, c) samples and (b, d) events during 2001–19. The left axis of (a–b) is for the average numbers (solid black lines) of HPCV samples or events, and the right axis is the ratio (bar) of HPCV to NCCV in terms of samples or events. The dashed red lines of (c–d) are the linear trend of the yearly variations (solid black lines), and all passed the significance test of $\alpha = 0.1$.

for reference. It is known that NCCV samples south of 40°N usually originate from subtropical jet streams, and they have a shorter lifetime and smaller radius than those originating north of 40°N (Kentarchos and Davies, 1998). Therefore, the main maximum cores of NCCV samples lie in the region 40°–55°N, and are likely to occur in regions of low terrain (Fig. 3). Specifically, NCCV samples are most concentrated over the Northeast China Plain, north of the Lesser Khingan Mountains, and the Sea of Okhotsk. The highest frequencies vary with seasons, showing an east-west orientation oscillation. The maximum frequency core gradually moves toward the continent in summer and to the North Pacific coast in winter. This zonal oscillation may be related to the strength and position of the upper-level jet streams (Nieto et al., 2005).

Since HPCV samples mostly occur in summer, the high-frequency region of HPCV samples is only located in the Northeast China Plain. It is difficult for the moisture currents

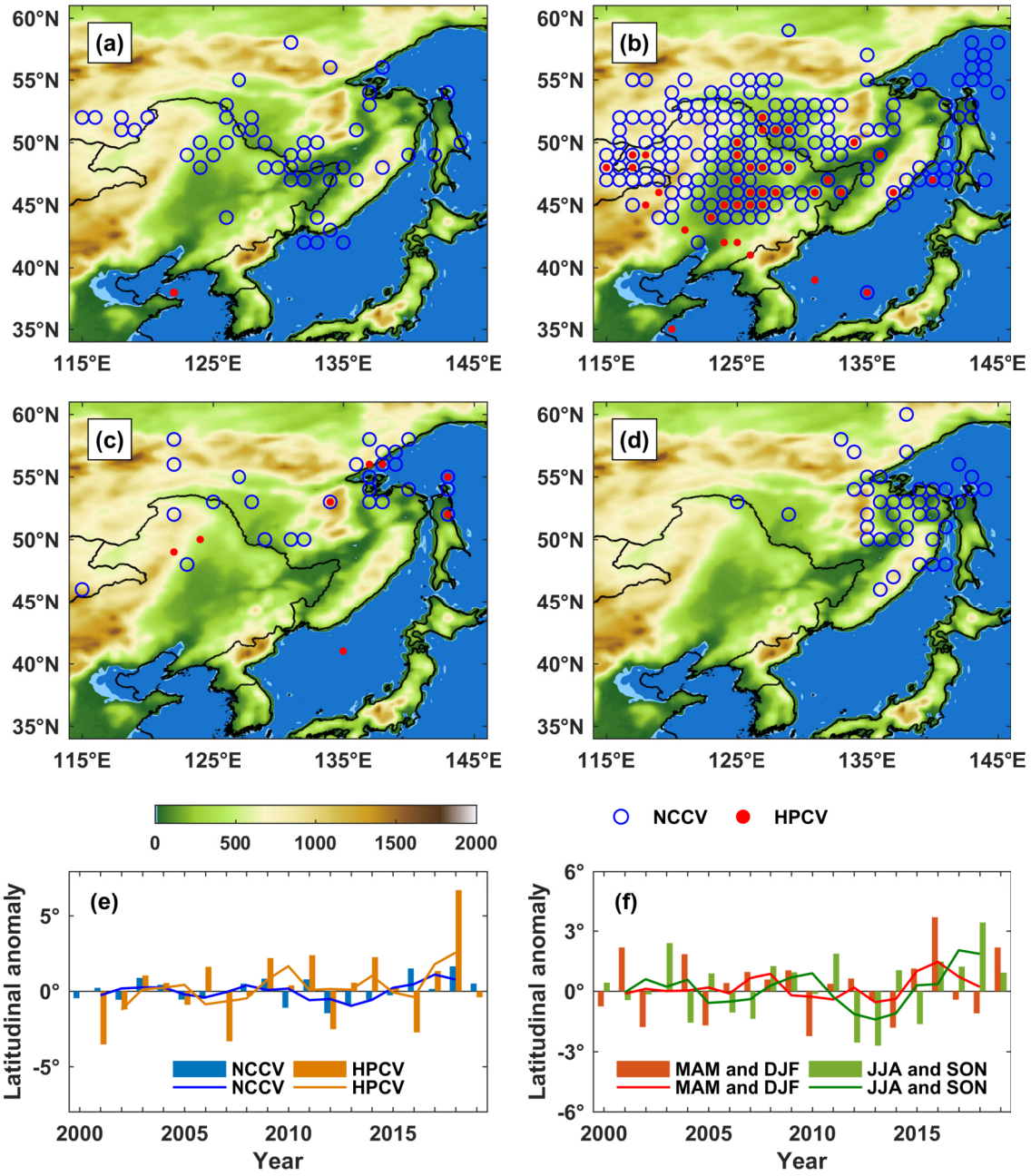


**Fig. 3.** (a–d) Spatial distribution of high frequencies of NCCV (blue circles) and HPCV (solid red dots) samples from 2000 to 2019 in (a) MAM, (b) JJA, (c) SON, and (d) DJF. A high frequency of NCCV (HPCV) samples is defined as the occurrence time is > 6 (2 for HPCV) in a certain season. The shading indicates terrain height (units: m). (e, f) Mean latitudinal anomaly of NCCV or HPCV samples from 2000 to 2019 and its three-point moving average (solid lines); (e) NCCV (blue) and HPCV (orange) samples, (f) NCCV samples in MAM and DJF (red) and JJA and SON (green).

to reach higher latitudes; therefore, the Sea of Okhotsk is no longer a maximum core of HPCV samples. The 20-year average position of HPCV samples is (46.36°N, 129.97°E), which is more southerly than that of the NCCV samples (49.91°N, 130.55°E).

Figure 3e shows the variations in the meridional departure of NCCV and HPCV centers from the average position. Before 2010, the central latitude of NCCV samples varies around the annual mean. The deviation after 2010 is larger than before, in the range of ±1.5°. By contrast, the deviation of HPCV centers is significantly larger than that of NCCV centers from 2000 to 2019. The latitudinal anomaly of HPCV centers is ±4° and the maximum deviation reached 6.76° in 2018.

The latitudinal change of NCCV centers in different seasons is investigated to explain the variations of deviation. As shown in Fig. 3f, before 2010, the direction of deviation in summer and autumn is opposite to that in spring and winter, leading to a small annual variation of NCCV occurrence latitudes. However, after 2010, the NCCV centers in different seasons no longer move in opposite directions. Therefore, the deviation of NCCV centers is larger. Similarly, since the proportion of HPCVs in NCCV samples is very low (only ~ 5%) in spring and winter, the latitudinal deviation for HPCVs in spring and winter is not enough to compensate for that in summer and autumn, which makes the annual latitudinal deviation of HPCV centers larger.

### 3.3. *Duration and Size*

The duration of HPCV events varies greatly (Fig. 4a). About 70.12% of the HPCV events last 3–5 days, and the longest process lasted 8.25 days. Seasonally, 22.22% of the HPCV events in MAM last five or more days, whereas the percentage is 34.48% in JJA, 17.78% in SON, and 50% in DJF, respectively. Therefore, HPCV events in winter are likely to be longer than in the other three seasons. Note that the duration of HPCV events is not equivalent to their lifetime. If the system moves in or out of the definition region, its lifetime is longer than detected. A more detailed classification is given in section 4.

Figure 4b illustrates the frequency distribution of the sizes of HPCV samples. The radii of HPCV samples are mostly concentrated in the 250–1000 km range, which accounts for about 79.17% of the total. The annual mean value of HPCV size is generally larger than NCCV (figures are given in the electronic supplementary material ). In winter, HPCV samples tend to have radii > 1000 km, indicating that an HPCV could develop to a larger size in the cold season. In summer, the percentage is the largest when the radius of HPCV samples is 250–500 km, which may be related to more convective events in summer, suppressing the increase in the area of the cold vortex (Porcù et al., 2007). Hu et al. (2010) pointed out that most NCCVs ranged between 500 and 1500 km, which is larger than our statistical results. This is because they defined the NCCV size by the longest dimension during its lifetime, whereas our method includes NCCV and HPCV samples in all synoptic hours.

The duration of an HPCV event is closely related to its average lifetime (Fig. 4c). When the HPCV events last < 4 days, the proportion of HPCV sizes ⩽ 500 km is the largest. However, when the HPCV events last longer (⩾ 5 days), HPCV sizes > 1000 km account for the largest proportion. Therefore, an HPCV event with a larger size lasts longer. For large HPCV samples, it takes more time for the system to develop and dissipate, so the duration is correspondingly longer.

## 4. Four Types of HPCV Events

HPCV events are divided into four types: move-in, genesis, move-out, and dissipation. The synoptic hour when an

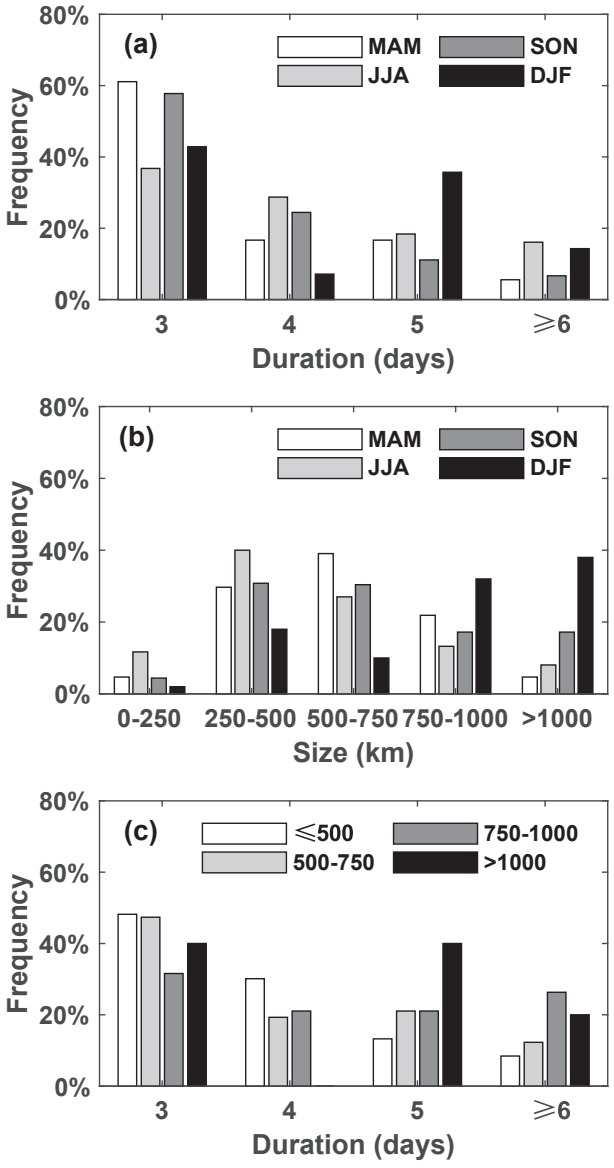


**Fig. 4.** Frequency distributions of (a) durations for HPCV events and (b) the sizes for HPCV samples in MAM, JJA, SON, and DJF. (c) Frequency distributions of durations as a function of average radii over the life of HPCV events.

HPCV event appears within the study region (35°–60°N, 115°–145°E) for the first (last) time is defined as the initial (final) time. The HPCV center is searched for within an extended region (20°–75°N, 100°–160°E) at the last (next) synoptic hour of the initial (final) time. If these two centers obtained at two consecutive synoptic hours fit the tracking criteria proposed in section 2.1, the HPCV event may be seen as the move-in (move-out) type. Otherwise, this event belongs to the genesis (dissipation) type. During the statistical analysis, an HPCV event may belong to both the move-in/genesis type and, concurrently, the move-out/dissipation type.

About 55.83% (51.53%) of HPCV events belong to the move-in (move-out) type, and the remaining half initiates (dissipates) within the definition region (Fig. 5). Move-in HPCV events mainly enter the region between 40° and 55° N near the western boundary. By contrast, the generated positions are widely distributed in all four quadrants, with 55.56% of HPCV events concentrated in the second quadrant. At the weakening stage, most HPCV events move out from the eastern boundary south of 55°N, whereas the positions of dissipation are mainly distributed in the first and fourth quadrants.

The tracks of HPCV events are also analyzed (figures omitted). Relative to their initial and final positions, HPCV events moved roughly eastward and southeastward. Qi et al. (1999) found that 81% of the cut-off lows in southern Australia moved either eastward or southeastward, whereas the remainder moved northward. Fang et al. (2021) considered the origins and movement velocities (distances) of NCCV events, dividing their activity paths into four types: eastward movement, southeastward long-distance movement, eastward less-movement, and southward less-movement. The proportion of the eastward movement type is the highest.

Figure 6a shows the duration of four HPCV types. For HPCV events that lasted 3–5 days, the proportion of the move-in type (78.02%) was higher than that of the genesis type (59.72%). The opposite results are obtained for HPCV events that lasted > 5 days, as move-in and genesis types accounted for 21.98% and 40.28%, respectively. Therefore, HPCV events that moved into the study region had a shorter duration than those initiated in the study region. However, there was no significant difference between HPCV events

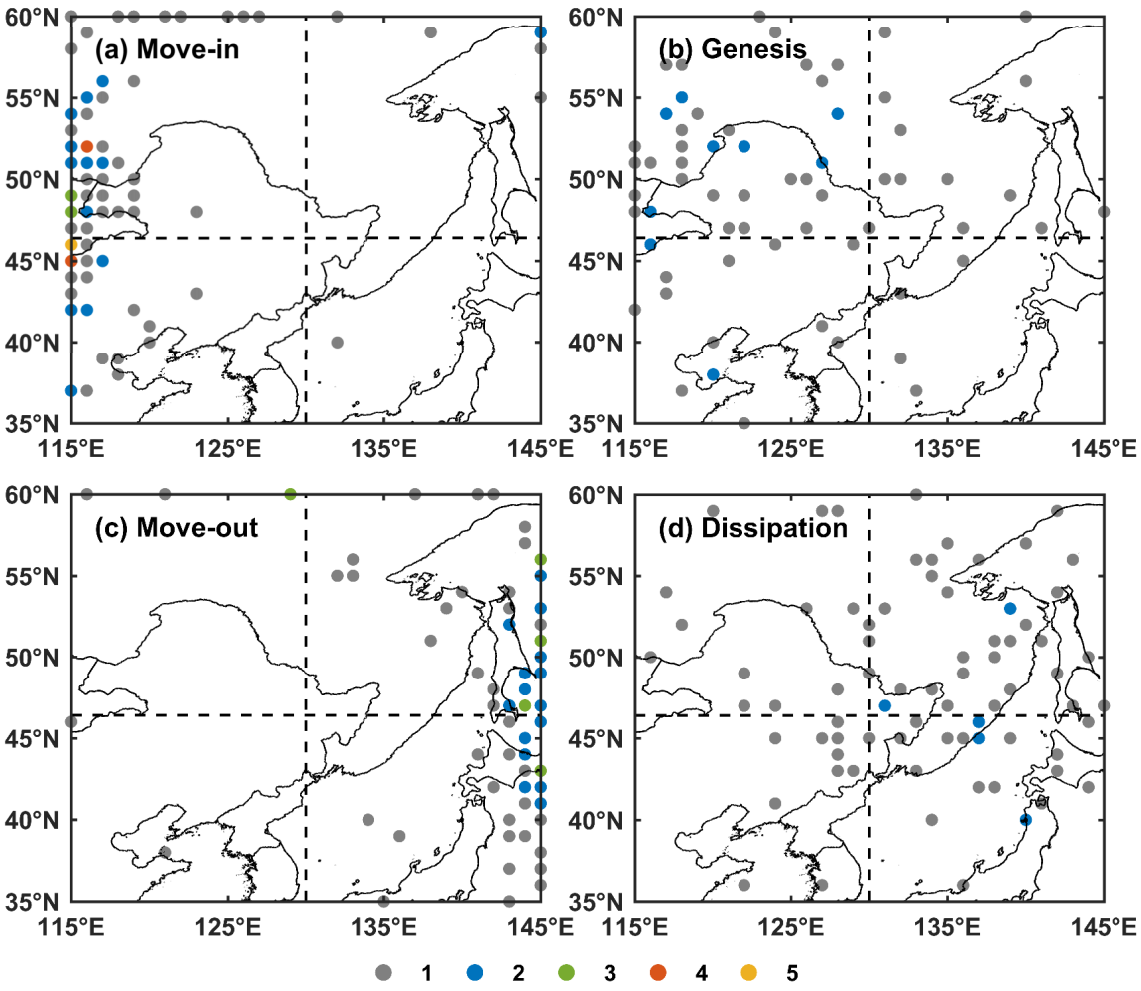


**Fig. 5.** (a, b) Initial and (c, d) final positions of HPCV events. The gray, blue, green, red, and yellow dots indicate the number of HPCV events is 1–5, respectively. The dashed lines divide the region into four quadrants based on the average position of HPCV events.

that moved out of the region or dissipated within the region, suggesting that the weakening stage of HPCV events has little effect on their duration. Similarly, there was little difference in the size of HPCV samples among the four HPCV types. (Fig. 6b).

## 5. Precipitation Characteristics of HPCV Samples

In this section, two parameters for HPCV samples, namely, the maximum 24-h accumulated precipitation (MAP) and 24-h accumulated precipitation core (APC), are discussed. MAP is defined as the average value of the top 10% of 24-h accumulated precipitation over the cold vortex rain area (i.e., the $P$ described in section 2.2). APC is defined as the precipitation centriod of the cold vortex rain area, where only grid points with 24-h accumulated precipitation $\geqslant$ 50 mm are included.

Figure 7 shows the temporal variations of annual or monthly mean MAP values. Obviously, the annual mean MAP has considerable inter-annual variability over the time period 2001–19, with an average of 67.24 mm. The greatest annual mean MAP values were 78.48 mm in 2006, 76.72 mm in 2016, and 74.50 mm in 2018. The years with low annual mean MAP were 2009 and 2011. Monthly variations of MAP values are also evident. The peak of 81.89 mm occurred in October. From January to March, the monthly MAP was low. In other months, MAP values fluctuated around the average.

APCs are mainly distributed in the Sea of Japan and its coastal land, showing a southwest- to northeast-oriented banded shape (Fig. 8a). This is because the ocean, with its abundant supply of moisture and the flat underlying surface, provides a better condition for rainstorms than the land surface.

There is a strong positive correlation between the locations of APCs and the HPCV centers. The correlation coefficients are 0.78 in latitude and 0.85 in longitude. However, this does not mean that APCs fall evenly around the HPCV centers. They are mostly concentrated within 2000 km southeast of the HPCV centers (Fig. 8b). When the precipitation value is large (>100 mm), APCs are mainly about 1000 km away from the center. The distance between the locations of APCs and the HPCV centers varies greatly, with the maximum and minimum distances of 3028.56 and 48.48 km, respectively.

It is worthy to note that the distributions of the APCs have seasonal differences. Specifically, in summer, 86.49% of the APCs are within 1200 km of the HPCV center (Fig. 8c), while in winter, 83.33% of the APCs are more than 1200 km

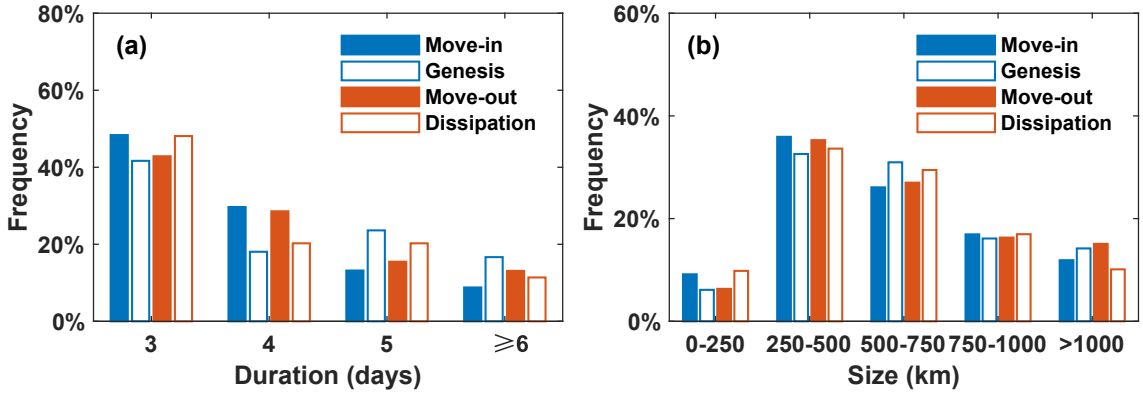


**Fig. 6.** Frequency distribution of (a) durations and (b) average sizes for the lifetime of four HPCV types.

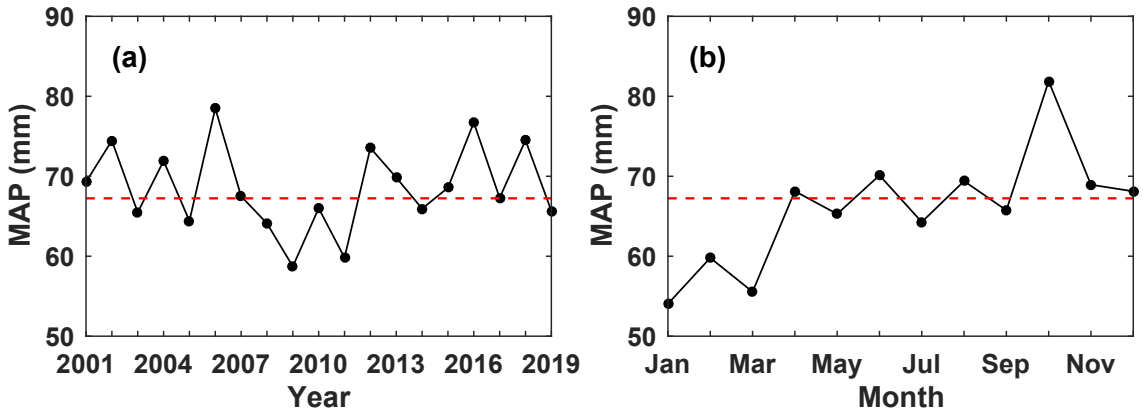


**Fig. 7.** (a) Yearly and (b) monthly variations of average MAP values (solid black line, units: mm) from 2001 to 2019 and their mean values (dashed red line).

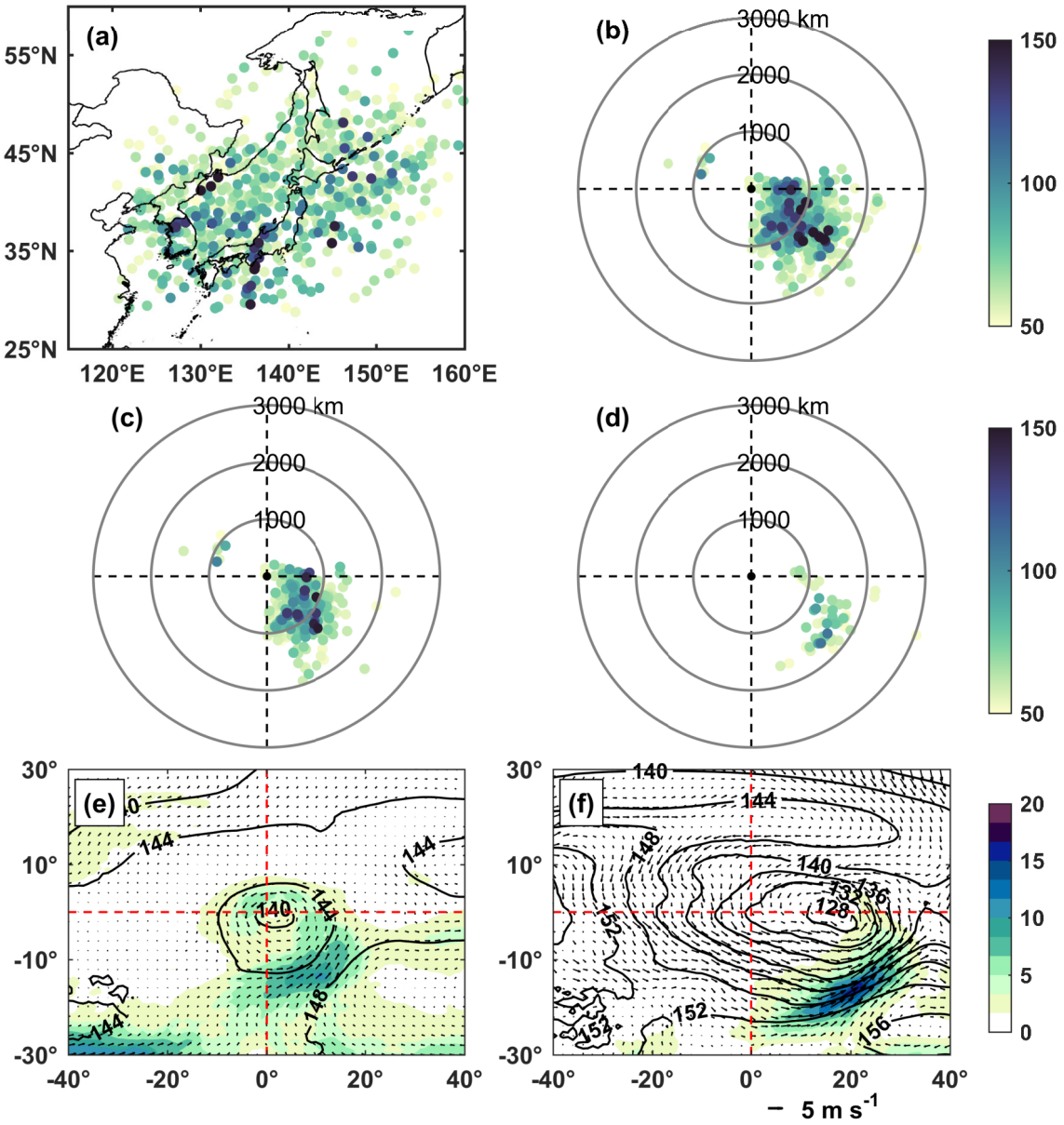


**Fig. 8.** (a) Geographical locations of the APCs, with colors indicating MAP (dots; units: mm). (b–d) Distribution of APCs (dots; units: mm) relative to the 500-hPa HPCV centers in (b) whole years, (c) JJA, and (d) DJF, respectively, within 19 years from 2001 to 2019. (e–f) 850-hPa composite circulations of HPCV samples from 2017 to 2019 in (e) JJA and (f) DJF. The black contours indicate geopotential height (units: dam), the arrows indicate wind (units: m $s^{-1}$), and the shading indicates water vapor flux [units: g (cm hPa s)$^{-1}$]. The dashed red lines divide the region into four quadrants based on the 500-hPa composite centers.

from the center (Fig. 9d). Therefore, the APCs in the cold season are farther from the center than those in the warm season. The reason is illustrated in Figs. 8e and 8f, which show the composites of 850-hPa water vapor flux, noting that low-level water vapor is an essential requirement for precipitation. Note that the origin (0°, 0°) indicates the composite center at 500 hPa and that the centers of the cold vortexes in the upper and lower levels do not coincide. There is an obvious water vapor band in the southeast of the HPCV system, and the distance between the water vapor band and the origin is closer in summer than in winter.

## 6. Conclusions and Discussions

Using the NCEP_FNL data and the IMERG precipitation product, 164 HPCV events were identified during 2001–2019. The basic characteristics of HPCVs are shown, and the main conclusions are as follows.

- The number of HPCV samples and events shows an upward linear trend from 2001 to 2019. There are more HPCV samples and events in summer than in the other three seasons.
- HPCV samples are frequently concentrated on the Northeast China Plain at 40°–55°N, which is related

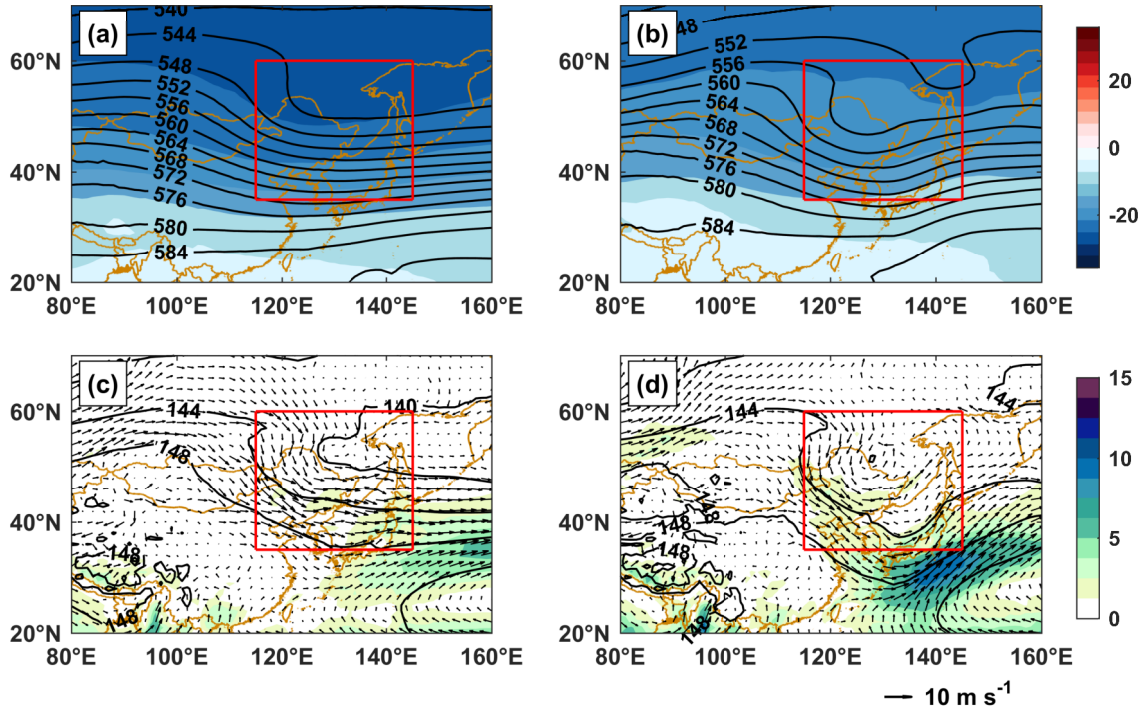


**Fig. 9.** Composite circulations of (a, c) NCCVs and (b, d) HPCVs from 2017 to 2019. (a, b) 500-hPa geopotential height (black contours; units: dagpm) and temperature (shading; units: °C). (b, d) 850-hPa geopotential height (black contours; units: dagpm), wind (arrows; units: m $s^{-1}$), and water vapor flux [shading; units: g (cm hPa s)$^{-1}$]. The red box indicates the study region.

to the moisture supply.

- Most HPCV events last 3–5 days. The HPCV events in winter are likely to last longer. 79.17% of HPCV samples have a radius between 250 and 1000 km. HPCV samples tend to have larger radii during the cold seasons. The duration of the larger-sized HPCV events is longer.
- About half of HPCV events move into (move out of) the definition region, and half initiate (dissipate) within the defined region. The initiation locations mainly range between 40° and 55°N near the western boundary, whereas the events tend to dissipate in the first and the fourth quadrants. HPCV events moving into the study region have a shorter duration than those initiated within this region.
- The APCs are mostly concentrated within 2000 km southeast of the HPCV systems, and they are farther from the center in the cold season than in the warm season.

To analyze the configuration that leads to HPCVs becoming distinct from general NCCVs, Fig. 9 compares the high- and low-level atmospheric circulations of NCCV and HPCV samples. There is little difference between NCCV and HPCV samples at 500 hPa. However, at 850 hPa, a significant water vapor band to the southeast of the system carries warm moisture from the southern seas to its center. Compared with the transportation of NCCV samples, HPCV samples have more abundant water vapor with values over 10 g (cm hPa s)$^{-1}$. Meanwhile, the trough associated with the HPCV samples is deeper, further strengthening the moisture transport from the south.

The strong low-level cyclonic circulation and sufficient moisture supply are favorable for the development from general NCCVs to HPCVs. However, the specific formation and development mechanisms from general NCCVs to HPCVs, are not studied in this paper. It is well known that NCCVs have a relatively uniform air mass in the upper and lower layers and that they do not cause heavy rainfall without interacting with other systems. On the other hand, extratropical cyclones are quasi-barotropic at the occlusion stage, with low pressure at lower levels and an overlapping cut-off low at upper levels, which begs the question, are the HPCVs accompanied by extratropical cyclones near the surface? The relationship between NCCVs, HPCVs, and extratropical cyclones still needs further study.

***Acknowledgements***. The authors thank the editors and three reviewers for their helpful comments and valuable suggestions, which improved the manuscript. This work was financially supported by the National Key R&D Program of China under Grant No. 2018YFC1507302, the National Natural Science Foundation of China under Grant No. 42175006, Jiangsu Youth Talent Promotion Project (2021-084), and the Basic Research Fund of CAMS under Grant No. 2020R002. The NCEP FNL Reanalysis dataset is available at https://rda.ucar.edu/datasets/ds083.2/index.html. The IMERG dataset is publicly available at https://disc.gsfc.nasa.gov/datasets/GPM_3IMERGHH_06/summary. The lists of 20-year

NCCVs and HPCVs are available for free at Zenodo via https://doi.org/10.5281/zenodo.5571340.

***Electronic supplementary material:*** Supplementary material is available in the online version of this article at https://doi.org/10.1007/s00376-022-2037-y.

## REFERENCES


Bai, R. H., and Y. G. Sun, 1997: The background analysis study of Meso-scale weather of the cold vortex in Northeast China. *Heilongjiang Meteorology*, (3), 6–7, 12. (in Chinese with English abstract)

Fang, Y. H., H. S. Chen, Y. Lin, C. Y. Zhao, Y. T. Lin, and F. Zhou, 2021: Classification of northeast China cold vortex activity paths in early summer based on *K*-means clustering and their climate impact. *Adv. Atmos. Sci.*, **38**(3), 400–412, https://doi.org/10.1007/s00376-020-0118-3.

Gimeno, L., R. M. Trigo, P. Ribera, and J. A. García, 2007: Editorial: Special issue on cut-off low systems (COL). *Meteorol. Atmos. Phys.*, **96**(1), 1–2. https://doi.org/10.1007/s00703-006-0216-5.

Guo, H., S. Chen, A. M. Bao, A. Behrangi, Y. Hong, F. Ndayisaba, J. J. Hu, and P. M. Stepanian, 2016: Early assessment of integrated multi-satellite retrievals for global precipitation measurement over China. *Atmospheric Research*, **176–177**, 121–133. https://doi.org/10.1016/j.atmosres.2016.02.020.

Guo, N. N., Y. S. Zhou, and L. M. Yang, 2021: Statistical analysis of Central Asian vortices and their influence on precipitation in Xinjiang. *Atmospheric Research*, **249**, 105327, https://doi.org/10.1016/j.atmosres.2020.105327.

Hosseini-Moghari, S.-M., and Q. H. Tang, 2022: Can IMERG data capture the scaling of precipitation extremes with temperature at different time scales. *Geophys. Res. Lett.*, **49**, e2021GL096392, https://doi.org/10.1029/2021GL096392.

Hsieh, Y. P., 1949: An investigation of a selected cold vortex over North America. *J. Meteor. Sci.*, **6**(6), 401–410, https://doi.org/10.1175/1520-0469(1949)006<0401:AIOASC>2.0.CO;2.

Hu, K. X., R. Y. Lu, and D. H. Wang, 2010: Seasonal climatology of cut-off lows and associated precipitation patterns over Northeast China. *Meteorol. Atmos. Phys.*, **106**, 37–48, https://doi.org/10.1007/s00703-009-0049-0.

Huang, W.-R., Y.-H. Chang, and P.-Y. Liu, 2018: Assessment of IMERG precipitation over Taiwan at multiple timescales. *Atmospheric Research*, **214**, 239–249, https://doi.org/10.1016/j.atmosres.2018.08.004.

Huang, X., and D. L. Li, 2020: Objective identification method and variation characteristics of the Northeast China cold vortex from May to August of 1979–2018. *Acta Meteorologica Sinica*, **78**(6), 945–961, https://doi.org/10.11676/qxxb2020.077. (in Chinese with English abstract)

Jiang, D. K., J. S. Wang, Q. Yan, P. Wang, and Y. Z. Lu, 2012: Climatic characters of northeast cold vortex and its effect on air temperature in Liaoning province from May to September during 1961–2010. *Journal of Meteorology and Environment*, **28**(2), 5–9, https://doi.org/10.3969/j.issn.1673-503X.2012.02.002. (in Chinese with English abstract)

Kalnay, E., and Coauthors, 1996: The NCEP/NCAR 40-Year reanalysis project. *Bull. Amer. Meteor. Soc.*, **77**(3), 437–472, https://doi.org/10.1175/1520-0477(1996)077<0437:TNYRP>2.0.CO;2.

Kentarchos, A. S., and T. D. Davies, 1998: A climatology of cut-off lows at 200 hPa in the Northern Hemisphere, 1990–1994. *International Journal of Climatology*, **18**(4), 379–390, https://doi.org/10.1002/(SICI)1097-0088(19980330)18:4<379::AID-JOC257>3.0.CO;2-F.

Ma, S. M., and C. W. Zhu, 2022: The cooling over Northeast Asia in June over the most recent decade: A possible response to declining Bering Sea sea ice in March. *Geophys. Res. Lett.*, **49**, e2022GL097773, https://doi.org/10.1029/2022GL097773.

Nieto, R., and Coauthors, 2005: Climatological features of cutoff low systems in the northern hemisphere. *J. Climate*, **18**(16), 3085–3103, https://doi.org/10.1175/JCLI3386.1.

Palmén, E., 1949: Origin and structure of high-level cyclones south of the: Maximum westerlies. *Tellus*, **1**(1), 22–31, https://doi.org/10.1111/j.2153-3490.1949.tb01925.x.

Porcù, F., A. Carrassi, C. M. Medaglia, F. Prodi, and A. Mugnai, 2007: A study on cut-off low vertical structure and precipitation in the Mediterranean region. *Meteorol. Atmos. Phys.*, **96**, 121–140, https://doi.org/10.1007/s00703-006-0224-5.

Qi, L., L. M. Leslie, and S. X. Zhao, 1999: Cut-off low pressure systems over southern Australia: Climatology and case study. *International Journal of Climatology*, **19**(15), 1633–1649, https://doi.org/10.1002/(SICI)1097-0088(19991219:15<1633::AID-JOC445>3.0.CO;2-0.

Sun, L., X. Y. Zheng, and Q. Wang, 1994: The climatological characteristics of northeast cold vortex in China. *Quarterly Journal of Applied Meteorology*, **5**(3), 297–303. (in Chinese with English abstract)

Sun, L., Q. Wang, and X. L. Tang, 1995: A composite diagnostic analysis of cold vortex of storm-rainfall and non-storm rainfall types. *Meteorological Monthly*, **21**(3), 7–10. (in Chinese with English abstract)

Sun, L., G. An, Y. Lian, B. Z. Shen, and X. L. Tang, 2000: A study of the persistent activity of northeast cold vortex in summer and its genral circulation anomaly charecteristics. *Acta Meteorologica Sinica*, **58**(6), 704–714, https://doi.org/10.3321/j.issn:0577-6619.2000.06.006. (in Chinese with English abstract)

Sun, L., G. An, Z. T. Gao, X. L. Tang, L. Ding, and B. Z. Shen, 2002: A composite diagnostic study of heavy rain caused by the northeast cold vortex over Songhuajiang-Nenjiang River basin in summer of 1998. *Journal of Applied Meteorological Science*, **13**(2), 156–162, https://doi.org/10.3969/j.issn.1001-7313.2002.02.003. (in Chinese with English abstract)

Wang, C. W., H. M. Xu, L. Ren, and L. Chen, 2012: The objective identification method of northeast cold vortex. *Journal of Meteorology and Environment*, **28**(2), 1–4, https://doi.org/10.3969/j.issn.1673-503X.2012.02.001. (in Chinese with English abstract)

Wen, D., Y. Li, D. L. Zhang, L. Xue, and N. Wei, 2018: A statistical analysis of tropical upper-tropospheric trough cells over the western north pacific during 2006–15. *J. Appl. Meteorol. Climatol.*, **57**(11), 2469–2483, https://doi.org/10.1175/JAMC-D-18-0003.1.

Xie, Z.-W., C. Bueh, L.-R. Ji, and S.-Q. Sun, 2012: The cold vortex circulation over northeastern China and regional rainstorm events. *Atmos. Ocean. Sci. Lett.*, **5**(2), 134–139, https://doi.org/10.1080/16742834.2012.11446979.

Yang, M. X., G. D. Liu, T. Chen, Y. Chen, and C. C. Xia, 2020: Evaluation of GPM IMERG precipitation products with the

point rain gauge records over Sichuan, China. *Atmospheric Research*, **246**, 105101, https://doi.org/10.1016/j.atmosres.2020.105101.

Ying, S., D. Y. Yuan, and S. F. Li, 2014: Comparative analysis of severe convective weather characteristics in different stages of Northeast China cold vortex. *Journal of Meteorology and Environment*, **30**(4), 9–18, https://doi.org/10.3969/j.issn.1673-503X.2014.04.002. (in Chinese with English abstract)

Zhang, C., Q. Zhang, Y. Wang, and X. Liang, 2008: Climatology of warm season cold vortices in East Asia: 1979–2005. *Meteorol. Atmos. Phys.*, **100**, 291–301, https://doi.org/10.1007/s00703-008-0310-y.

Zhang, J. K., W. S. Tian, M. P. Chipperfield, F. Xie and J. L. Huang, 2016: Persistent shift of the Arctic polar vortex towards the Eurasian continent in recent decades. *Nature Climate Change*, **6**, 1094–1099, https://doi.org/10.1038/nclimate3136.

Zhang, L. X., and Z. C. Li, 2009: A summary of research on cold vortex over northeast China. *Climatic and Environmental Research*, **14**(2), 218–228, https://doi.org/10.3878/j.issn.1006-9585.2009.02.11. (in Chinese with English abstract)

Zheng, X. Y, T. Z. Zhang, and R. H. Bai, 1992: *Rainstorm in Northeast China*. China Meteorological Press, 19–43.